CU-2172-28

A PHENOMENOLOGICAL MODEL FOR TRANSIENT DEFORMATION BASED ON STATE VARIABLES

M. S. Jackson, C. W. Cho, P. Alexopoulos, H. Mughrabi, and Che-Yu Li

Department of Materials Science and Engineering
Cornell University
Ithaca, NY 14853
USA

DISCLAIMER

ABSTRACT

The state variable theory of Hart, while providing a unified description of plasticity-dominated deformation, exhibits deficiencies when it is applied to transient deformation phenomena at stresses below yield. It appears that the description of stored anelastic strain is oversimplified.

Consideration of a simple physical picture based on continuum dislocation pileups suggests that the neglect of weak barriers to dislocation motion is the source of these inadequacies. An appropriately modified description incorporating such barriers then allows the construction of a macroscopic model including transient effects.

Although the flow relations for the microplastic element required in the new theory are not known, tentative assignments may be made for such functions. The model then exhibits qualitatively correct behavior when tensile, loading-unloading, reverse loading, and load relaxation tests are simulated.

Experimental procedures are described for determining the unknown parameters and functions in the new model.

1. INTRODUCTION

Several approaches have recently been proposed to describe the non-elastic deformation of crystalline solids.[1-5] These theories employ a mechanical equation of state, in that the instantaneous response of a solid to an applied mechanical constraint is calculated using a number of internal parameters (state variables) which together contain the relevant effects of thermal and deformation history.

The great advantage of state variable theories is that the specimen behavior can be calculated for any deformation path for which the evolution laws for the state variables are known. Thus such (traditionally) distinct phenomena as creep, constant strain-rate extension, and load relaxation can be handled in a unified manner.

To be computationally useful, such a theory must adequately represent real materials behavior over some range of temperature and of deformation history. In addition, the number of state variables must be reasonably small and their values subject to experimental measurement. Whether <u>any</u> state variable theory satisfies a given set of constraints of this type can, of course, only be determined by experiment.

For nonrecoverable deformation (plastic flow), the state variable approach suggested by Hart[6,7] appears adequate to meet these criteria. This theory, originally developed to explain load relaxation experiments near the yield stress, has been extended by the addition of time-dependent but recoverable (anelastic) deformation. In this form, it has enjoyed considerable success in describing a variety of deformation modes, such as creep, load relaxation, and constant extension rate tensile tests in the plastic region. As discussed below, a number of real effects of interest seem not to be contained in the present theory. These include various manifestations of microplasticity at stresses well below yield, and the Bauschinger effect.

This paper represents an attempt to extend Hart's approach to include these effects. Hart's theory, and its successes and limitations, are first described. A microscopic description of recoverable strain is then developed which, while not unique, reproduces the linear anelasticity and other features of Hart's model. The underlying assumptions of this description are examined, and factors affecting the inadequacies discussed above are identified.

On the basis of this microscopic description modifications to Hart's model are proposed. These modifications include the addition of a microplastic flow element, the characteristics of which are to be determined experimentally.

By assigning constitutive relations to this element which are consistent with the known plastic flow behavior, however, it is possible to examine the behavior of the model under various loading histories. It is found that the new model can exhibit transient behavior similar to that which is observed experimentally but not contained in Hart's theory.

Finally, experiments to validate the model and to measure the parameters of interest are proposed.

As will be seen, Hart's theory divides nonelastic deformation into two components. The plastic component is time-dependent and permanent in that it is not recoverable by unloading. The anelastic component, by contrast, represents time-dependent deformation involving stored strain which is in principle recoverable at zero applied stress.

In what follows, we shall find that some types of materials behavior not involving action of the "plastic element" in the state variable theories do not fall within the description of anelasticity given above. These include flow-like effects which may lead to deformation which is essentially unrecoverable at zero applied stress. We shall employ the term "transient deformation" for all nonelastic effects not involving the plastic element. "Microplasticity" will be used to denote "transient" effects which are flow-like.

2. BASIC STATE VARIABLE MODEL

The description of nonelastic grain matrix deformation in terms of Hart's state variable theory has been presented elsewhere.[6,7] A brief description is given here.

The model employs three deformation elements, representing stored anelastic strain (a-element), plastic deformation ($\dot{\alpha}$-element), and glide friction ($\dot{\varepsilon}$-element). A schematic representation of the combination of these elements is given in Figure 1; it will be seen that the constraint equations are

$$\dot{\varepsilon} = \dot{a} + \dot{\alpha} \tag{1}$$

and

$$\sigma = \sigma_a + \sigma_f \tag{2}$$

where σ, σ_a, and σ_f are the applied stress, back stress due to stored anelastic strain, and glide friction stress; and $\dot{\varepsilon}$, $\dot{a}$, and $\dot{\alpha}$ are the nonelastic strain rate, anelastic strain rate, and plastic deformation rate.

For the a-element, stress and stored strain are related in a linear fashion through a modulus M:

$$\sigma_a = Ma \ ; \tag{3}$$

the friction stress is found to be related to the strain rate by

$$\dot{\varepsilon} = \dot{a}^* \ (\sigma_f/G)^M \tag{4}$$

where G is the modulus of rigidity, $\dot{a}^*$ a rate parameter, and $M \simeq 7.5$.

Flow in the plastic element is given by

$$\ln \ (\sigma^*/\sigma_a) = (\dot{\varepsilon}^*/\dot{\alpha})^\lambda \tag{5}$$

with scaling

$$\dot{\varepsilon}^* = (\sigma^*/G)^m f \ e^{-Q/RT} \ ; \tag{6}$$

work-hardening and recovery are incorporated by

$$\frac{d\ln\sigma^*}{dt} = \Gamma \ (\sigma^*, \sigma_a) \ \dot{\alpha} - R \ (\sigma^*, T) \tag{7}$$

In this equation, σ^* is the hardness (similar to a yield stress), $\dot{\varepsilon}^*$ a rate parameter, $\lambda \simeq 0.15$, $m \simeq 4.5$, f some characteristic frequency, Q generally equal to a self-diffusion activation energy, and R generally negligible at moderate homologous temperatures. The work-hardening function Γ has been found to be[7,8]

$$\Gamma = \left(\frac{\sigma_a}{\sigma^*}\right)^{\beta/\sigma^*} \left(\frac{\beta}{\sigma^*}\right)^{\delta} \qquad (8)$$

where β and δ are materials constants.

This model has been shown to describe the tensile, load relaxation, and creep behavior of a number of crystalline solids under unidirectional loading when plastic flow predominates. In the form given here, it does not address the question of effects due to grain boundary sliding. Certain real matrix processes, such as large-scale thermal recovery and dynamic strain-aging, are either neglected or only tentatively incorporated (e.g. by the R-term in Equation 7) as well.

For a certain range of temperature and deformation, these effects sre expected to be small. We take the attitude that materials under these conditions exhibit a basic matrix behavior, which is to be represented by the state variable theory. Grain boundary effects could then be accounted for by addition to the matrix equations, a problem which has received some attention.[1,6,9] Explicit inclusion of recovery and strain-aging may be possible by time-dependent changes in the matrix state variables.

Within these restrictions, the above model seems to represent the plastic behavior of materials quite adequately. There are, however, significant disagreements with experiment for deformation at stresses less than yield.

Figure 2a is a schematic representation of materials behavior during a constant extension rate tensile test carried into the plastic region. Because

of the nature of the plastic flow element (Equation 5), which is dictated by the results of load relaxation studies, the predicted onset of yield behavior is more rapid than in real materials, particularly for annealed specimens.

Figure 2b depicts constant extension rate loading and unloading below yield. In this case, the model behavior is dictated by the linear anelasticity of the a-element, giving a simple stress-strain loop of the type shown. By contrast, real materials deviate from this behavior, both during loading at some fraction of the yield stress and during unloading as the stress approaches zero. In addition, some nonrecoverable strain may be accumulated even when the peak stress is well below yield.

These problems would seem to be related; in both cases one observes some flow-like behavior, or microplasticity, under conditions where plastic flow is not expected. Although the differences between theory and experiment are of little importance on a strain scale appropriate to plastic effects, they represent significant deviations from linear anelasticity.

Larger differences are evident when one examines loading histories involving reversal of the applied stress. Real materials generally show a Bauschinger effect, in that a specimen which has been plastically deformed in, e.g. compression exhibits more strain during subsequent tensile loading than during compressive reloading. This additional strain is manifested at quite low stress levels (Figure 2c).

In contrast, Hart's model is almost completely symmetric in these two cases. Because of the weak dependence of the glide stress σ_f on strain rate (Equation 4), some anelastic strain can be trapped after unloading to zero stress, and this strain is released upon reverse loading. For realistic materials parameters, however, this asymmetry is much less than the observed Bauschinger strain.

Since all of the above discrepancies occur below macroscopic yield, they are presumably associated with the representation of stored strain by a simple linear element in Hart's theory. We wish to develop a more complete theory which can account for such effects in a unified way. We will refer to these as transient effects, in that plastic flow as represented by the $\dot{\alpha}$-element is not involved, although the microplastic and Bauschinger strains are not of course fully recoverable upon unloading of the specimen.

3. MICROMECHANICAL DESCRIPTION OF THE STATE VARIABLE THEORY

From a phenomenological point of view any number of approaches might be used to represent more correctly the transient behavior. One could employ, for example, some sort of variable modulus in a differential form of Equation 3, or introduce additional flow elements into the diagram. A micromechanical description of Hart's model would clearly be of great use as a guide.

Hart's state variable model was developed from rather general consideration of the constraints on such an approach.[11] It is essentially phenomenological in that the basic flow relations have been determined by experiment; no first-principles calculation of materials behavior has been attempted.

It is, however, possible to establish a connection between several broad features of the model and microscopic processes.[12] Essentially, one represents the specimen by a collection of two-dimensional slip zones bounded by strong barriers to dislocation motion. Dislocation pileups between the barriers are then treated using continuum theory.[13] The anelastic strain (a) as a function of pileup stress (σ_a) is then found from the net dislocation moment per zone, under the assumption that dislocations move freely between the barriers.

In this picture, the plastic strain rate ($\dot{\alpha}$) is due to leakage of the leading dislocation through the barrier, the strength of which is a function of hardness (σ^*), and restoration of the pileup by operation of a dislocation source. The zone and pileup are shown in Figure 3. For this simple picture, the anelastic modulus

$$M = \frac{G}{\pi l^2 \eta} \tag{9}$$

where l is half the slip zone length and η is the number of slip zones per unit projected area.

If the glide friction stress is assumed to be a functionof dislocation velocity, σ_f will vary over the slip zone. In general, the dislocation velocity

distribution is different for changes in the pileup structure (which give $\dot{a}$) and for barrier leakage (which gives $\dot{\alpha}$). However, the variation of σ_f with velocity is such that the average glide stress is essentially a function of nonelastic strain rate ($\dot{\varepsilon} = \dot{a} + \dot{\alpha}$).

This pileup picture, then, reproduces the rheological diagram, Figure 1. As noted above, however, the flow relations for the $\dot{\alpha}$ and $\dot{\varepsilon}$ elements must be imposed in order to represent the full materials behavior.

The relation for the plastic element, Equation 5, is most clearly manifested during load relaxation at high homologous temperatures when glide friction is unimportant. When recovery and strain-aging effects can be neglected, constant-hardness curves of this form are observed in a wide variety of materials. We take, therefore, Equation 5 and the scaling and work-hardening relations, Equations 6-8, as the proper description of dislocation leakage through the strong barriers and of the evolution of σ^* and $\dot{\varepsilon}^*$.

The nature of the dislocstion glide friction is seen during load relaxation tests at low homologous temperatures.[14] Under these conditions, the pileup stress σ_a is very close to σ^* and dislocation motion is essentially controlled by the $\dot{\varepsilon}$-element, which behavior is found experimentally to be given by Equation 4.

With the specification of the flow laws Equations 4-8, this dislocation pileup description appears to be the simplest micromechanical picture of the features of Hart's state variable model. The deficiencies which have been identified in this model suggest that the pileup picture is oversimplified; identification of the shortcomings of the pileup picture on physical grounds may then provide useful guidance in the construction of a more realistic macroscopic theory. We turn now to consideration of effects which, in real crystals, would change the pileup description.

First, we have assumed the existence of well defined dislocation pileups on single slip planes. Although such structures are observed in many materials, they are not seen in others where cross-slip can easily take place. It is clear, however, that some sort of dislocation pileup is necessary for macroscopic yield behavior to occur. Dislocations on nearby slip planes will interact, and whether a pileup is a simple two-dimensional structure or an extended dislocation cloud the essential features of stress concentration leading to barrier penetration will remain. We expect, therefore, that replacement of the present slip zone by an extended slip region would not modify the resulting constitutive relations.

Second, we have postulated a single zone length and barrier strength throughout the specimen. This is clearly an approximation, but is quite possibly justified for the strong barriers which control plastic flow. This is because the relevant microstructure is the result of prior plastic deformation, and we would expect the self-correcting nature of the work-hardening process to limit structural inhomogeneity.

There remains, however, the possibility of weaker barriers to free dislocation motion within the idealized slip zone. If we identify the strong barriers with dislocation cell walls, these weaker barriers would be isolated dislocation tangles or second-phase particles. The existence of such barriers modifies the pileup picture presented above, and therefore the associated state variable theory.

Consider, for instance, the simple example of Figure 4, where we have assumed a uniform distribution of small barriers over the slip zone. Under loading, dislocations will pile up in front of the weak barriers as shown. At sufficiently high stress, leakage through the small barriers will occur, contributing to the overall pileup across the zone against the strong barriers.

It is clear that the configuration of Figure 4 will exhibit effects in loading and unloading below macroscopic yield which are of the sort desired. For example, upon loading a linear stress-strain region (representing pileup between weak barriers) will be followed by a region of additional microplastic strain (representing leakage through the weak barriers). In addition, upon unloading to zero stress anelastic strain due to the large pileup can be trapped in the forward direction by the weak barriers. This strain will contribute to the Bauschinger effect upon reverse loading.

Another attractive feature of this formulation is that the plastic behavior is unmodified. At high stresses the pileups in front of the weak barriers are fully developed, and plastic strain is impeded only by the strongest barriers.

Introduction of such a barrier structure within the slip zone does not, of course, uniquely define a macroscopic model. We would require a detailed knowledge of the distribution of weak barrier strengths and spacing, and of barrier passage kinetics, which is not available. Many of the essential features of the corresponding macroscopic model are, however, derivable from this physical picture, a topic to which we now turn.

4. MODIFIED STATE VARIABLE THEORY

In Hart's theory the transient deformation properties are described by the state of anelastic strain. This stored strain (a) is a good state variable, since the single type of dislocation pileup it represents has a unique stress-strain relationship.

In the physical picture of Figure 4 this is no longer true; there are two types of pileups contributing to the stored strain. In order to construct the simplest possible macroscopic theory which can reflect the considerations of the preceding section we will require two state variables for the stored strain, and thus two anelastic elements of different moduli. A flow element (microplastic element) for weak barrier passage is also needed.

The arrangement of these three elements is dictated by Figure 4. Since leakage of dislocations through the weak barriers contributes to the long-range pileup distribution, the microplastic element must be in parallel with the long-range anelastic spring. It is also necessary that the effective force for barrier passage represent the fact that such leakage is resisted by the long-range pileup stress.

These considerations are incorporated in the diagram of Figure 5. Here the former anelastic element has been replaced by the elements labelled a_1, a_2, and $\dot{\alpha}_2$. The long-range dislocation pileup distribution is represented by the a_1-element. The short-range pileups are represented by the a_1- and a_2-elements acting together; the net force for passage through the small barriers is then represented by the stress in the a_2-element. The constraint equations implied by the diagram are

$$\sigma_a = \sigma_f + \sigma_a = \sigma_f + \sigma_{a_1} + \sigma_{a_2} \tag{10}$$

and

$$\dot{\varepsilon} = \dot{\alpha}_1 + \dot{a}_1 = \dot{\alpha}_1 + \dot{\alpha}_2 + \dot{a}_2 \tag{11}$$

which replace Equations 1 and 2.

The constitutive relations for the new anelastic elements are

$$\sigma_{a_1} = M_1 a_1 \tag{12}$$

and

$$\sigma_{a_2} = M_2 a_2 \tag{13}$$

where M_1 is primarily a function of the strong barrier spacing and $M_1 + M_2$ is a function of the weak barrier spacing. The microplastic strain rate $\dot{\alpha}_2$ will depend on σ_{a_2}.

For the plastic element ($\dot{\alpha}_1$) and the glide friction stress element ($\dot{\varepsilon}$) no modification is necessary. Thus Equations 4-8 can be taken (with appropriate addition of subscripts) as the governing relations. This provides a complete description of the new state variable model, except for the kinetics and evolution laws for the microplastic element ($\dot{\alpha}_2$).

These relations are not known a priori. Within the above framework, however, they can be determined experimentally. Procedures for determining the characteristics of the $\dot{\alpha}_2$-element will be discussed below.

Nonetheless, it is of interest to examine the qualitative behavior of this model under various loading histories to determine if the effects discussed previously are exhibited. For this purpose it is necessary to make a tentative assignment of the flow and evolution laws for the $\dot{\alpha}_2$-element.

We take as a guide the physical picture of Figure 4 and the known relations from Hart's theory. For the $\dot{\alpha}_2$-element, we will assume the relation

$$\ln\left(\frac{\sigma_2^*}{\sigma_{a_2}}\right) = \left(\frac{\dot{\varepsilon}_2^*}{\dot{\alpha}_2}\right)^{\lambda_2} \tag{14}$$

the same form as that for the plastic element, since both processes involve leakage through barriers. We will also assume a scaling relation

$$\dot{\varepsilon}_2^* = (\sigma_2^*/G)^{m_2} f_2 \, e^{-Q/RT} \qquad (15)$$

by analogy with Equation 6.

There remains the problem of an evolution law for the microhardness parameter σ_2^*. For plastic flow, the evolution of the hardness σ_1^* is given by a work-hardening function (Equations 7 and 8) which essentially describes changes in the relevant microstructure under plastic deformation.

For the microplastic case, the situation is somewhat different. We may presume that the weak barriers have a distribution of strengths, and that as the weakest barriers are overcome the flow will be controlled by successively stronger barriers. The evolution of σ_2^* is then a sampling effect rather than the result of work-hardening.

Consider, for example, the behavior of the dislocation pileups during a tensile test. Initially, the weakest barriers are effective and the strain is anelastic (modulus $M_1 + M_2$). As leakage through the weakest barriers begins, microplastic strain will accumulate. As the stress σ_{a_2} rises, further leakage will be resisted by stronger barriers within the slip zone. Thus during loading σ_2^* can be expected to increase with σ_{a_2}.

When the stress is decreasing (during load relaxation or unloading) microplastic strain in the forward direction should be controlled by the strongest barriers sampled during loading; that is, σ_2^* should be a constant for this case. When σ_{a_2} changes sign, however, which in general may occur during unloading before zero applied stress is reached, dislocations will pile up in the reverse direction against the weakest barriers. Some minimum value σ_{20}^* is then appropriate until these barriers are overcome and σ_2^* once again begins to increase.

Evidently, the evolution of σ_2^* can be quite complex. For the desired simulations, we make a tentative choice of the evolution law which may be adequate

for the present purpose:

$$\dot{\sigma}_2^* = 0 \qquad \text{for } |\sigma_{a_2}| \text{ decreasing;} \tag{16a}$$

$$\sigma_2^* = \sigma_{20}^* \qquad \text{for } |\sigma_{a_2}| \leq K\,\sigma_{20}^* \text{ and } |\sigma_{a_2}| \text{ increasing} \tag{16b}$$

$$\sigma_2^* = \left|\frac{\sigma_{a_2}}{K}\right| \qquad \text{for } |\sigma_{a_2}| > K\,\sigma_{20}^* \text{ and } |\sigma_{a_2}| \text{ increasing.} \tag{16c}$$

We emphasize that these relations are chosen only for the rather simple loading histories to be considered in the next section. Factors affecting σ_2^* will be considered further in Section 6. We also observe that, even with these restrictions, there is no particular reason to expect σ_2^* to bear a simple linear relation to σ_{a_2}, as would be implied if the factor K were a constant in Equation 16c. In fact, preliminary experimental evidence suggests that K is given by

$$K = e^{-C\sigma_{a_2}} \tag{17}$$

where the factor C is found to be numerically very close to

$$C = \frac{1}{\sigma^*}\,\frac{M_2}{M_1+M_2} \tag{18}$$

Whether Equation 18 has any physical significance is not, at the moment, understood.

With the caveat that the relations for the microplastic element, Equations 14-18, are tentative, we have now specified all of the necessary laws for the new state variable theory.

5. COMPARISON OF MODELS BY SIMULATION

Simulation of a number of loading histories was carried out using a computer program which has been described elsewhere.[15] For Hart's model, parameters were employed which are appropriate to a work-hardened specimen of high purity Al at room temperature. For the new model, parameters were carried over from Hart's theory whenever possible. For the other parameters, estimates were made on the basis of preliminary experimental work. The values of the parameters used are given in Table 1.

The program simulates deformation of a specimen in an actual testing machine when the sample dimensions and crosshead extension rate are given. Machine compliance is considered; the results can then be displayed as stress vs. strain or in other convenient form. The specimens were assumed to be of 3.90 cm (1.54 in.) initial length and 0.293 cm^2 (0.0453 in^2) initial area. Extension rates were 0.051 cm/min (0.02 in/min) or zero depending on the phase of the test.

All strains presented inFigs. 6-10 are nonelastic strains, although specimen elasticity is of course included in the simulations. Thus, for example, the vertical portions of the stress-strain curves represent stress ranges over which linear elasticity is dominant.

Simulation of a constant extension rate tensile test into the plastic region is shown in Figure 6. Above about 30 MPa microplastic strain due to the $\dot{\alpha}_1$-element is evident, giving the gradual transition to yield which is desired. After yield, the two models behave similarly since the deformation is dominated by the $\dot{\alpha}_1$-element (plastic element).

Figure 7 shows the result of simulations of repeated loading and unloading below yield. Hart's model exhibits repetitive behavior since there is no mechanism for accumulation of strain below yield after the initial loading.

For the new model, the shape of the stress-strain loop is much more physical. In addition, microplastic strain is accumulated over successive cycles. This process will eventually saturate, in agreement with experiment.

The curves of Figure 8 show the behavior of samples immediately reloaded in tension or compression after plastic deformation in compression. The new model exhibits a strong Bauschinger effect due to the release of stored strain from the a_1-element which was accumulated in compression. This additional strain is not recoverable upon unloading, as shown by the figure.

It is important to examine the behavior of the new model in a situation for which Hart's theory provides an adequate description, in order to determine if the modifications we have introduced have left the successes of Hart's theory intact. For this purpose we have simulated several load relaxation tests using the parameters of Table 1.

Figure 9 shows the results for Hart's model. The upper curve is a simulation of load relaxation from a fully plastic state, showing the typical behavior of the $\dot{\alpha}_1$-element. The lower curves are "transient" load relaxation tests, in which a sample of the same hardness σ_1^* is reloaded to just below the plastic region.

Experimentally, it si found that such transient curves merge with the fully plastic curve at lower strain rates and follow it thereafter.[16] (This is a manifestation of equation of state behavior.) The form of the transient curve predicted by Hart's theory, which is essentially dictated by the $\dot{\epsilon}$-element, is however not in accord with experiment for Al.

For the new model, the situation is much improved. The plastic relaxation in Figure 10 (upper curve) is essentially the same as in Hart's model. (This demonstrates that the introduction of microplastic effects does not disturb the plastic behavior, where Hart's theory has been shown to be sufficient.) The form of the transient behavior, however, is now determined by the $\dot{\alpha}_2$-element; the results are in much better accord with experiment.[16]

6. DISCUSSION

The preceding simulations indicate that the new theory, while preserving the successful features of Hart's model, can exhibit much more realistic behavior under reverse loading and in the stress range below yield. Whether the new theory can quantitatively represent these effects, of course, can only be determined by experiment. The procedures by which the necessary parameters and unknown relations can be measured are outlined in Section 7; such an effort is now in progress. Accepting for the sake of argument, however, the essential correctness of the new model, there remain several issues worthy of discussion.

The first concerns the meaning of the various types of strain which have been described in the preceding treatment. Previous authors[1] have divided strain into three components—an elastic part (reversible upon unloading to zero stress, and time-independent when inertial effects can be neglected), an anelastic part (reversible but time-dependent), and a plastic part (time-dependent and unrecoverable). With the addition of an elastic spring in series with the rheological diagram of Figure 1, each of these strain components corresponds to a particular deformation element in Hart's theory.

This correlation, while convenient, is not crucial to a meaningful theory of deformation. Indeed, even in Hart's theory it is only approximately true; in any real experiment the time available to recover strain stored in the a-element is finite, and some stored strain (trapped by the kinetics of the $\dot{\varepsilon}$-element) would be "plastic strain" by the criteria of the preceding paragraph.

In the new theory, this correlation is much less direct. All strains in the a_1-, a_2-, and $\dot{\alpha}_2$-elements are in principle recoverable (since at zero applied stress all strain rates are exactly zero only when $a_1 = a_2 = 0$, which imples $\alpha_2 = 0$); this perhaps justifies the use of the term "transient deformation." Of course, the kinetics of the flow elements insure that in a real experiment,

some of the strain in these elements will contribube to apparent "plastic strain."

For convenience, we have used the terms anelastic, microplastic, and plastic rather loosely to describe the general behavior of the varius elements. In Section 4 we have also associated these ideas with particular micromechanisms, although this was done only as a guide to developing the new model. That these terms do not have an unambiguous operationsl definition should not be disturbing, since this merely indicates that real materials deformation is sufficiently complex to require complex models for its representation. The important question is whether the parameters of the model are susceptible to measurement in the laboratory, and this, as will be seen in Section 7, should be possible.

The second issue of interest is the behavior of the $\dot{\varepsilon}$-element. As noted previously, the kinetics of this element can be found from load relaxation behavior at low homologous temperatues; it is found that the behavior follows Equation 4. Experience has shown, however, that Equation 4 with a constant value of the rate parameter $\dot{a}^*$ is not a good representation of glide friction at all levels of applied stress. Instead, it appears that glide is much easier after yield than during initial loading even in a high-purity solid. This effect was taken into account in the simulations of Section 5, where a larger value of $\dot{a}^*$ was used for load relaxation (Figures 9 and 10) than for the other curves (see Table 1).

Physically, this effect may be understood, for example, as a manifestation of breakaway from solute atmospheres when the dislocation velocity increases abruptly at yield. One would then expect a rapid increase in $\dot{a}^*$ near yield, with a slow recovery by diffusive processes at low strain rates. With such variation the state variable models would exhibit yield drop and strain-aging effects.

The detailed behavior of the glide friction stress under these conditions

is not known. The approach we have used in Section 5 is consistent with the general behavior, however, and should not affect the validity of the comparison between the two models. Although this approximate approach to the glide friction is adequate for many purposes, further experimental work on this question is clearly needed.

Finally, we would like to consider briefly the evolution law for the microplastic hardness parameter σ_2^*. A tentative form for this relationship, which is presumably due to sampling of the weak barrier distribution by the small dislocation pileups as σ_{a_2} changes, was given in Equations 16-18.

We emphasize again that such a relationship is highly simplified, and probably cannot hold for more general loading histories than were considered in Section 5. The evolution of σ_2^* will depend not only on the distribution of weak barriers but on the initial distribution of the small pileups as well. This pileup distribution will be different, for example, for reloading after complete unloading and after partial unloading. Whether such effects can be conveniently incorporated into the framework of the new model is a question to be resolved by experiment.

We have also ignored the possibility of changes in the small barrier structure due to deformation. One might expect, for example, some sort of work-hardening effect in microplasticity of the weak barriers are dislocation structures.

The incorporation of these matters into a macroscopic theory of deformation would seem to require a more satisfactory microscopic picture than that presented in Section 3. For the moment we take a phenomenological approach, and now turn to the question of experimental tests of the new model.

7. PROPOSED EXPERIMENTAL TESTS OF THE NEW MODEL

The characteristics of the new model should be capable of direct experimental verification by straightforward techniques.[6] For example, as noted previously the behavior of the $\dot{\varepsilon}$-element (Equation 4) can be determined by load relaxation at low homologous temperatures. At high homologous temperatures, load relaxation in the plastic region will measure the parameters of the $\dot{\alpha}_1$-element (Equation 5); a series of such tests will give the scaling relationship (Equation 6). Finally, a constant extension rate tensile test will allow the determination of the work-hardening coefficients (Equation 8).

The combined anelastic modulus $M_1 + M_2$ is directly measurable from the initial slope of the stress-nonelastic strain curve during a tensile test.[17] Separate estimation of M_1 requires observation of the stress-nonelastic strain relationship when the $\dot{\alpha}_2$-element is fully saturated. Depending on materials parameters, this may occur during loading just before yield, near the end of unloading, or during reverse loading.

Given the above parameters, it is generally possible to calculate σ_{a_2} and $\dot{\alpha}_2$ during tensile and load relaxation tests. Load relaxation well below yield should be dominated by the $\dot{\alpha}_2$-element, and it should be straightforward to determine if the behavior is described by Equation 14. Whatever relationship is found to be correct, a series of such tests should give the necessary scaling and evolution equations for completion of the model.

Preliminary results on Al indicate that Equations 14 and 15 are obeyed. The relationship between σ_{a_2} and σ_2^* during loading may then be found from the load relaxation tests, by comparing σ_{a_2} at the moment the crosshead is stopped with the σ_2^* found during relaxation. In addition, knowledge of the parameters of Equation 15 allows calculation of σ_2^* from the values of σ_{a_2} and $\dot{\alpha}_2$ during loading in the microplastic range. These measurements will allow the determination of the value or functional form of the factor $K = |\sigma_{a_2}|/\sigma_2^*$ (Equation 16).

This completes the description, in general terms, of the experimental program necessary to compare quantitatively the new model with real materials behavior. The details of these calculations, and the results of such an effort now underway, will be given in a forthcoming paper.

8. CONCLUSIONS

The state variable theory of Hart, while providing a unified description of plasticity-dominated deformation, exhibits deficiencies when it is applied to transient deformation phenomena at stresses below yield. It appears that the description of stored anelastic strain is oversimplified.

Consideration of a simple physical picture based on continuum dislocation pileups suggests that the neglect of weak barriers to dislocation motion is the source of these inadequacies. An appropriately modified description incorporating such barriers then allows the construction of a macroscopic model including transient effects.

Although the flow relations for the microplastic element required in the new theory are not known, tentative assignments may be made for such functions. The model then exhibits qualitatively correct behavior when tensile, loading-unloading, reverse loading, and load relaxation tests are simulated.

Experimental procedures have been described for determining the unknown parameters and functions in the new model. Such experiments are now being carried out.

ACKNOWLEDGEMENT

This work was supported by the United States Department of Energy.

REFERENCES

1. E. W. Hart, Che-Yu Li, H. Yamada, and G. Wire, in Constitutive Equations in Plasticity, A. S. Argon, ed., MIT Press (Cambridge), 1975, p. 149.
2. E. T. Onat and F. Fardshiseh, ORNL-4783 (1972).
3. U. F. Kocks, A. S. Argon, and M. F. Ashby, Thermodynamics and Kinetics of Slip, Progress in Materials Science 19, B. Chalmers et. al., eds., Pergamon Press (Oxford), 1975.
4. A. Miller, J. Eng. Mat. Tech. 98, 97 (1976).
5. D. N. Robinson, ORNL-TM-5110 (1975).
6. E. W. Hart, J. Eng. Mat. Tech. 98, 193 (1976).
7. F. H. Huang, H. Yamada, and Che-Yu Li, in Characterization of Materials for Service at Elevated Temperatures, G. V. Smith, ed., Series MPC-7, ASME (New York), 1978, p. 83.
8. G. L. Wire, F. V. Ellis, and Che-Yu Li, Acta Met. 24, 677 (1976).
9. J. M. Roberts, Acta Met. 15, 411 (1967).
10. E. W. Hart, Acta Met. 15, 1545 (1967).
11. E. W. Hart, Acta Met. 18, 599 (1970).
12. E. W. Hart, paper presented at the AIME annual meeting, 1977 (unpublished).
13. J. P. Hirth and J. Lothe, Theory of Dislocations, McGraw-Hill (New York), 1968.
14. F. H. Huang, F. V. Ellis, and Che-Yu Li, Met. Trans. 8A, 699 (1977).
15. V. Kumar, F. Huang, S. Mukherjee, and Che-Yu Li, EPRI final report, contract RP697-1, Department of Materials Science and Engineering, Cornell University, Ithaca, NY (1979).

16. E. W. Hart and H. D. Solomon, Acta Met. 21, 295 (1973).

17. P. Alexopoulos, C. W. Cho, C. P. Hu, and Che-Yu Li, "Determination of Anelastic Modulus for Several Metals," to be published.

TABLE 1

Parameters Used in the Simulations of Section 5

Hart's model symbol	new model symbol	equation	value
M	$(M_1 + M_2)$	3	5.90×10^5 MPa (85.5×10^6 psi)
-	M_1	12	1.12×10^5 MPa (16.3×10^6 psi)
-	M_2	13	4.77×10^5 MPa (69.2×10^6 psi)
σ^*	σ_1^*	5	60.1 MPa (8.72×10^3 psi)
$\dot{\varepsilon}^*$	$\dot{\varepsilon}_1^*$	5,6[a]	4.80×10^{-16} sec^{-1}
λ	λ_1	5	0.15
m	m_1	6	4.8
β	β	8	103 MPa (1.5×10^4 psi)
δ	δ	8	2.8
M	M	4	7.8
dislocation glide constant[b]		4	3.62×10^5 sec^{-1} MPa$^{-7.8}$ (5×10^{-12} sec^{-1} psi$^{-7.8}$)
dislocation glide constant[c]		4	8.68×10^{-10} sec^{-1} MPa$^{-7.8}$ (1.2×10^{-26} sec^{-1} psi$^{-7.8}$)
-	σ_{20}^*	14,16	0.414 MPa (60.0 psi)
-	$\dot{\varepsilon}_{20}^*$	14,15[a]	3.20×10^{-23} sec^{-1}
-	λ_2	14	0.15
-	m_2	15	7.26
Young's modulus		-	5.86×10^4 MPa (8.5×10^6 psi)

[a] The specification of a single pair σ^*, $\dot{\varepsilon}^*$ defines the scaling relationship of equation 6 or 15 at constant temperature.

[b] Equal to $\dot{a}^*/G^M$; value for load relaxation. See text.

[c] Equal to $\dot{a}^*/G^M$; value for other simulations. See text.

FIGURE CAPTIONS

Figure 1: Rheological diagram representing the deformation elements of Hart's state variable model.

Figure 2: Schematic representation of real materials behavior (dashed curves) and the predictions of Hart's model (solid curves) for various loading histories.

(a) Constant extension rate tensile test to yield.

(b) Loading and unloading below yield.

(c) Reloading in the forward direction (left-hand curves) and in the reverse direction (right-hand curves) following plastic deformation.

Figure 3: Net lineal dislocation density $n(x)$ across a slip zone under an applied stress in the continuum approximation.

Figure 4: Effect of the introduction of weak barriers to dislocation motion on the dislocation pileup.

Figure 5: Rheological diagram representing the deformation elements of the new state variable model.

Figure 6: Simulation of a constant extension rate tensile test to yield using Hart's model (solid curve) and the new model (dashed curve). Parameters are given in Table 1.

Figure 7: Simulation of repeated loading and unloading below yield using Hart's model (solid curve) and the new model (dashed curve). Parameters are given in Table 1.

Figure 8: Simulation of constant extension rate tensile deformation of a sample previously deformed plastically in compression (Bauschinger effect) using Hart's model (solid curve) and the new model (dashed curve). Parameters are given in Table 1.

Figure 9: Simulation of load relaxation from the fully plastic region (upper curve) and from just below the yield stress (lower curves) using Hart's model. Parameters are given in Table 1.

Figure 10: Simulation of load relaxation from the fully plastic region (upper curve) and from just below the yield stress (lower curves) using the new model. Parameters are given in Table 1.

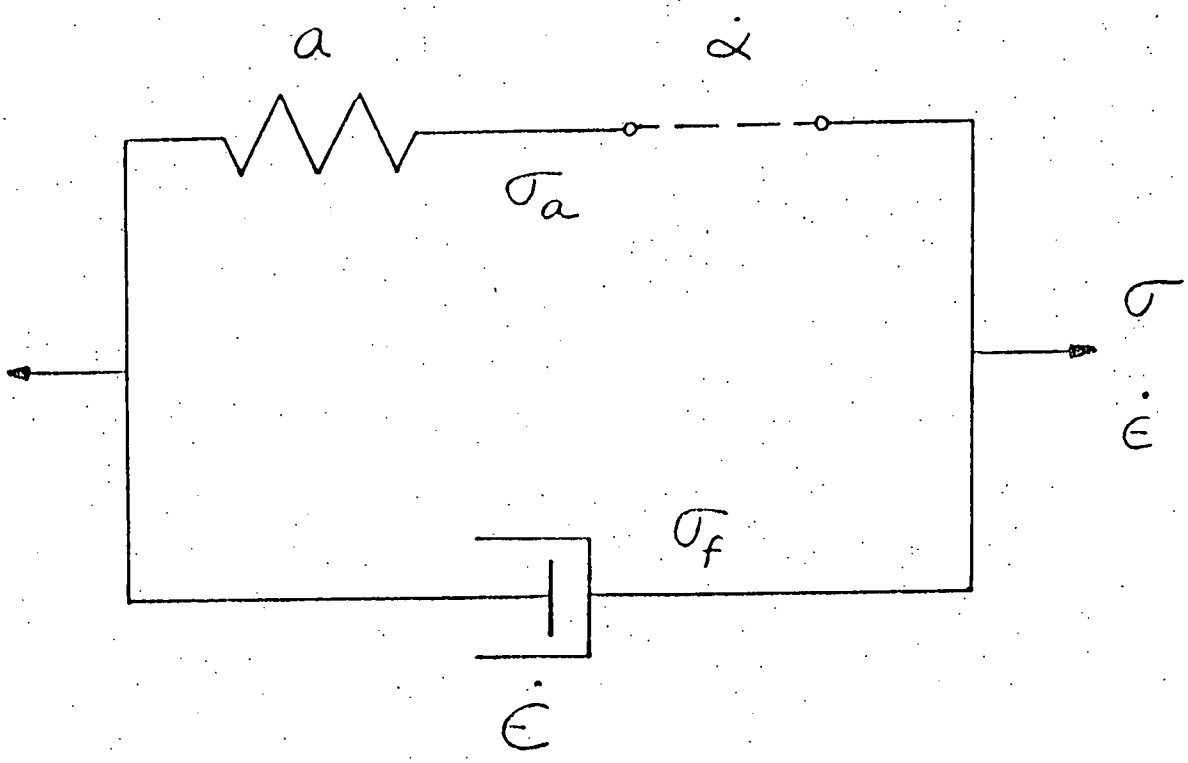

FIGURE 1

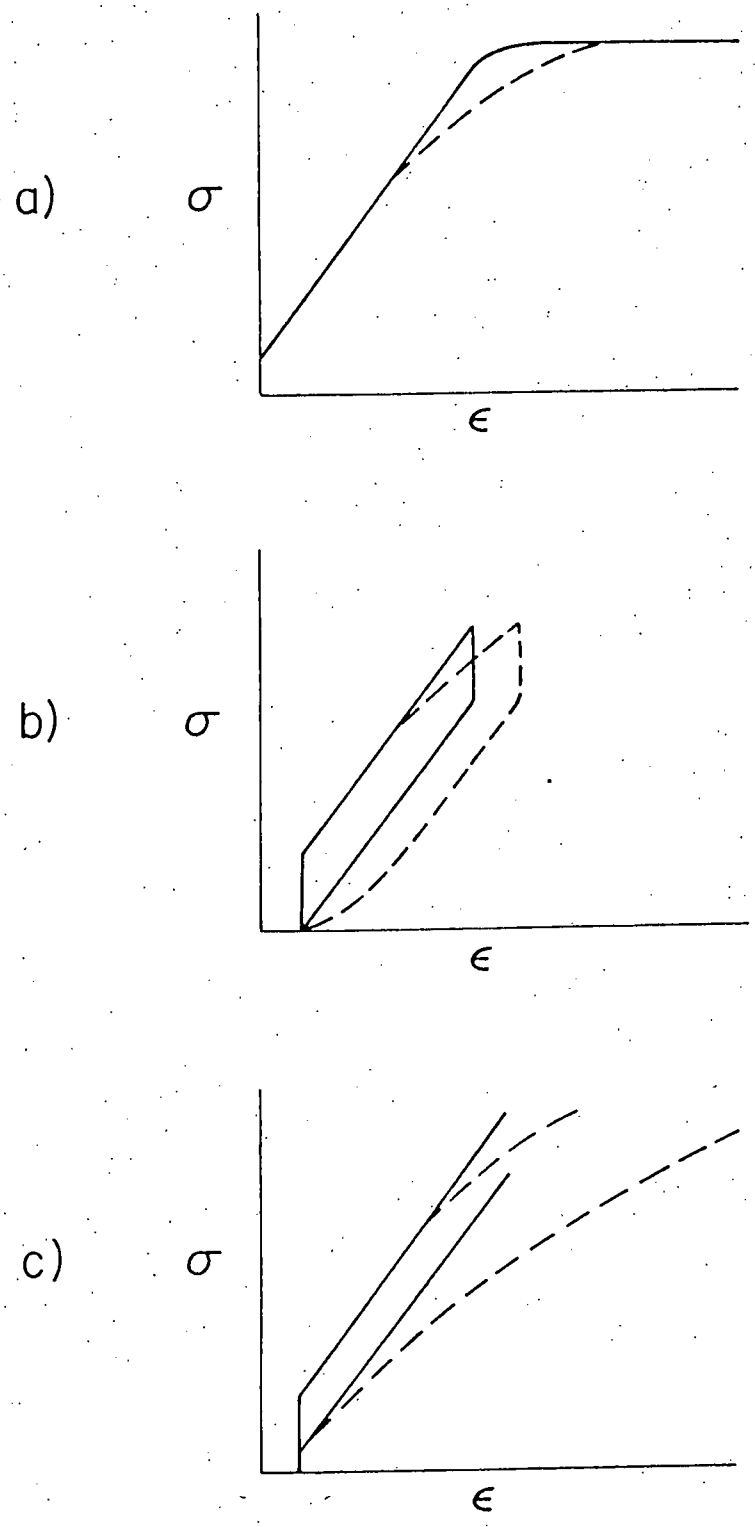

FIGURE 2

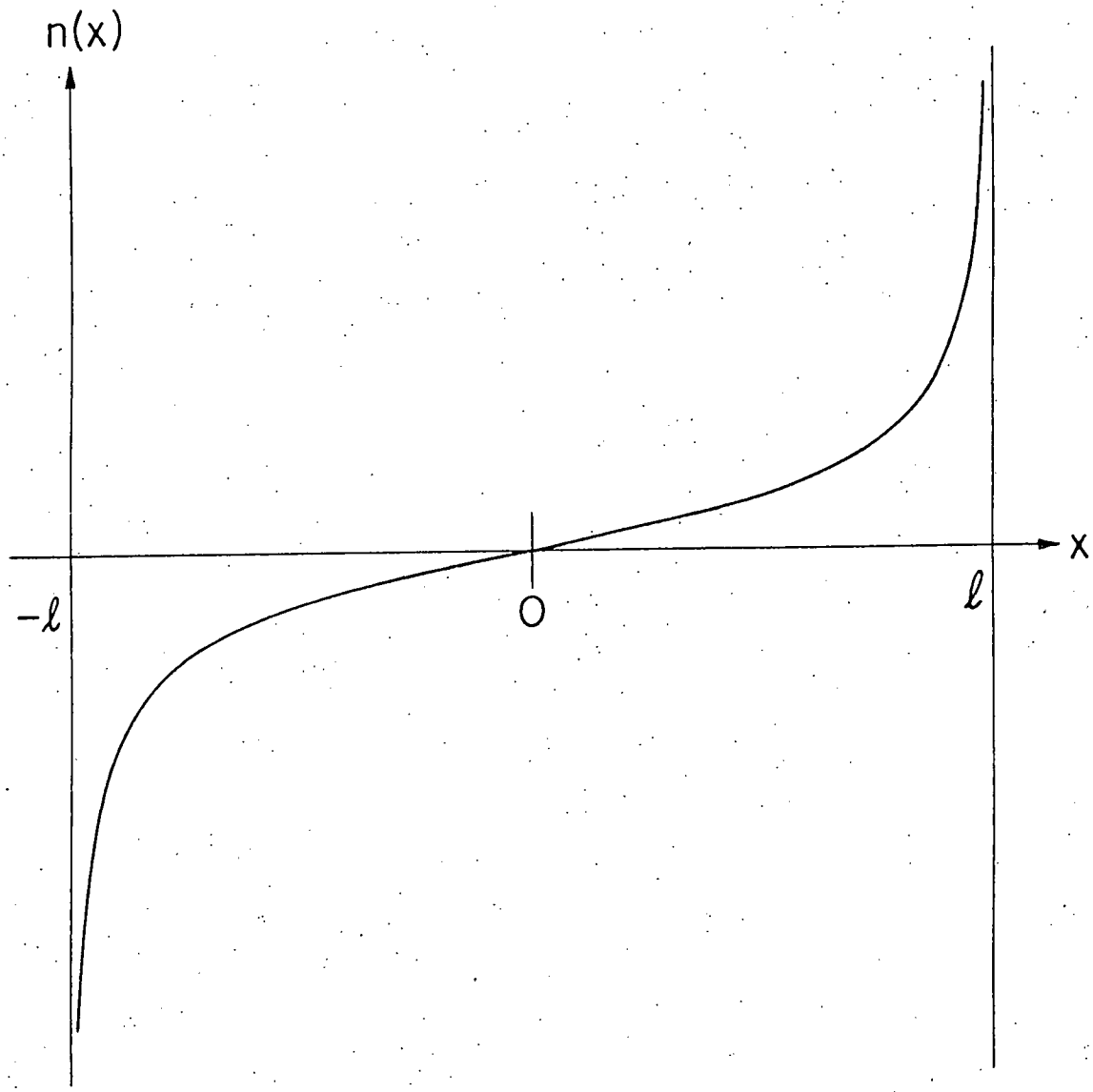

FIGURE 3

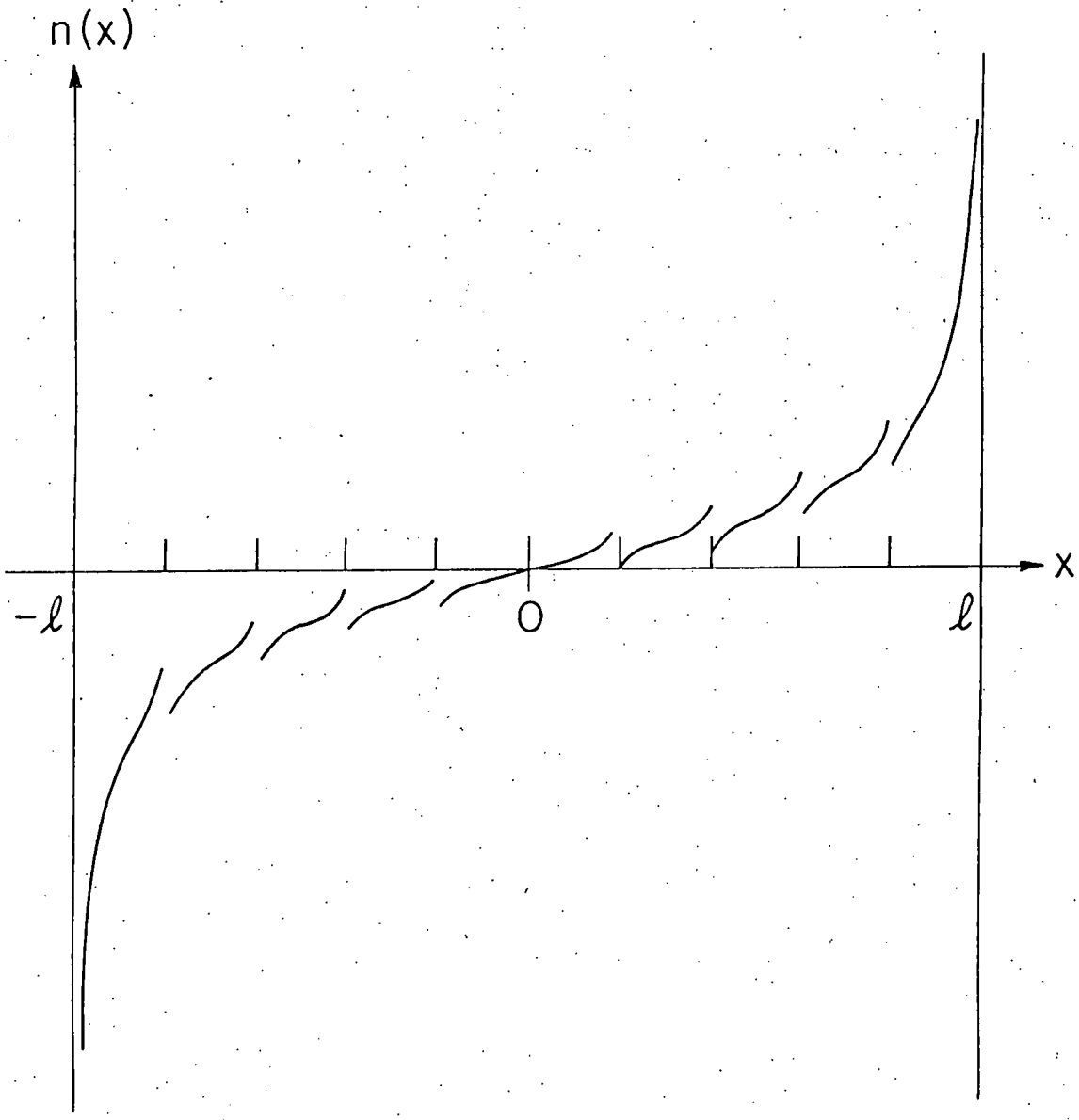

FIGURE 4

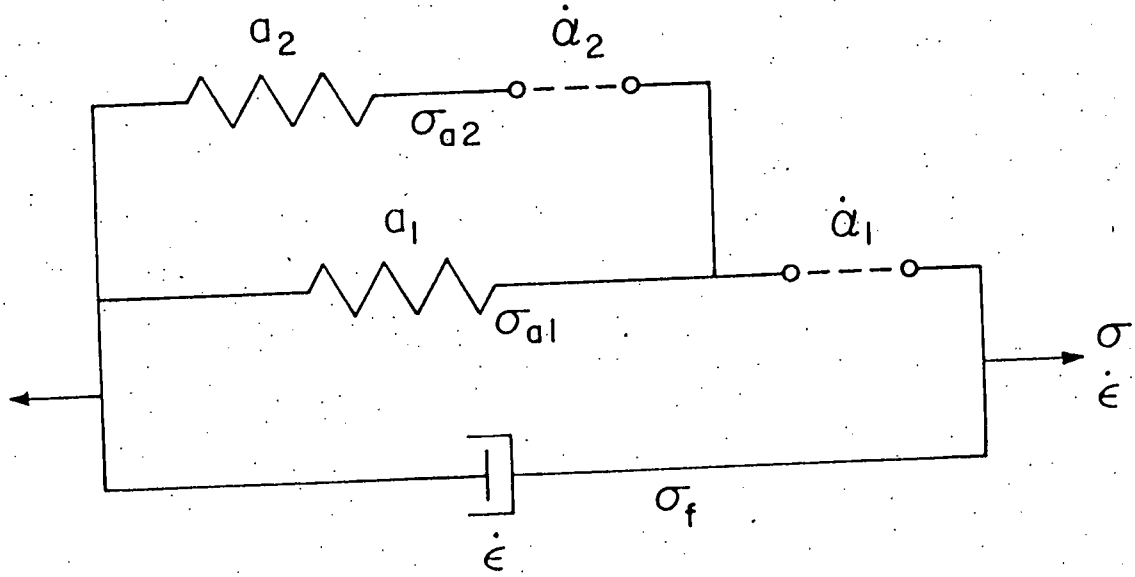
a_2
$\dot{a}_2$
σ_{a2}
a_1
$\dot{a}_1$
σ_{a1}
σ
$\dot{\epsilon}$
σ_f
$\dot{\epsilon}$

FIGURE 5

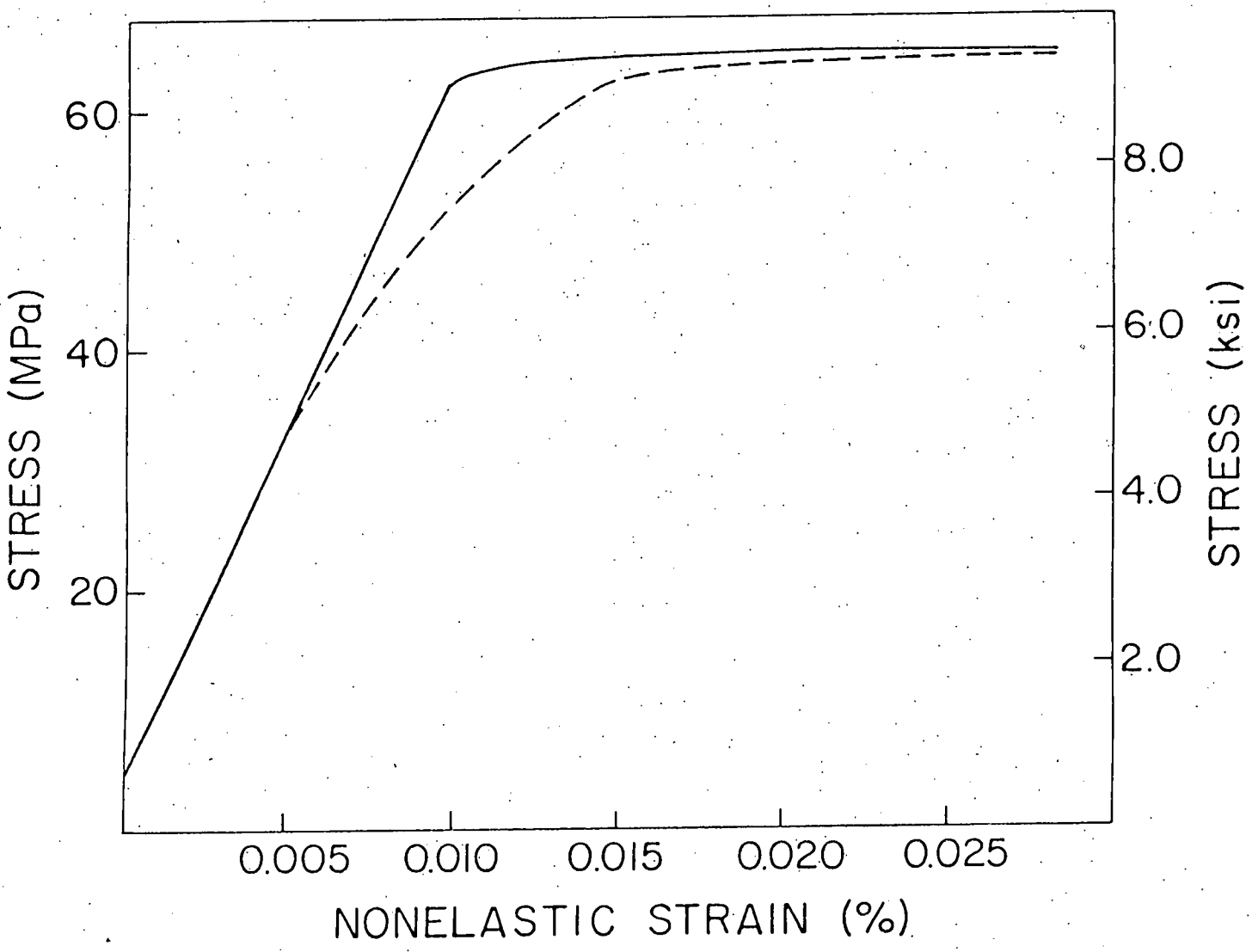
60
40
20
STRESS (MPa)
8.0
6.0
4.0
2.0
STRESS (ksi)
0.005
0.010
0.015
0.020
0.025
NONELASTIC STRAIN (%)

FIGURE 6

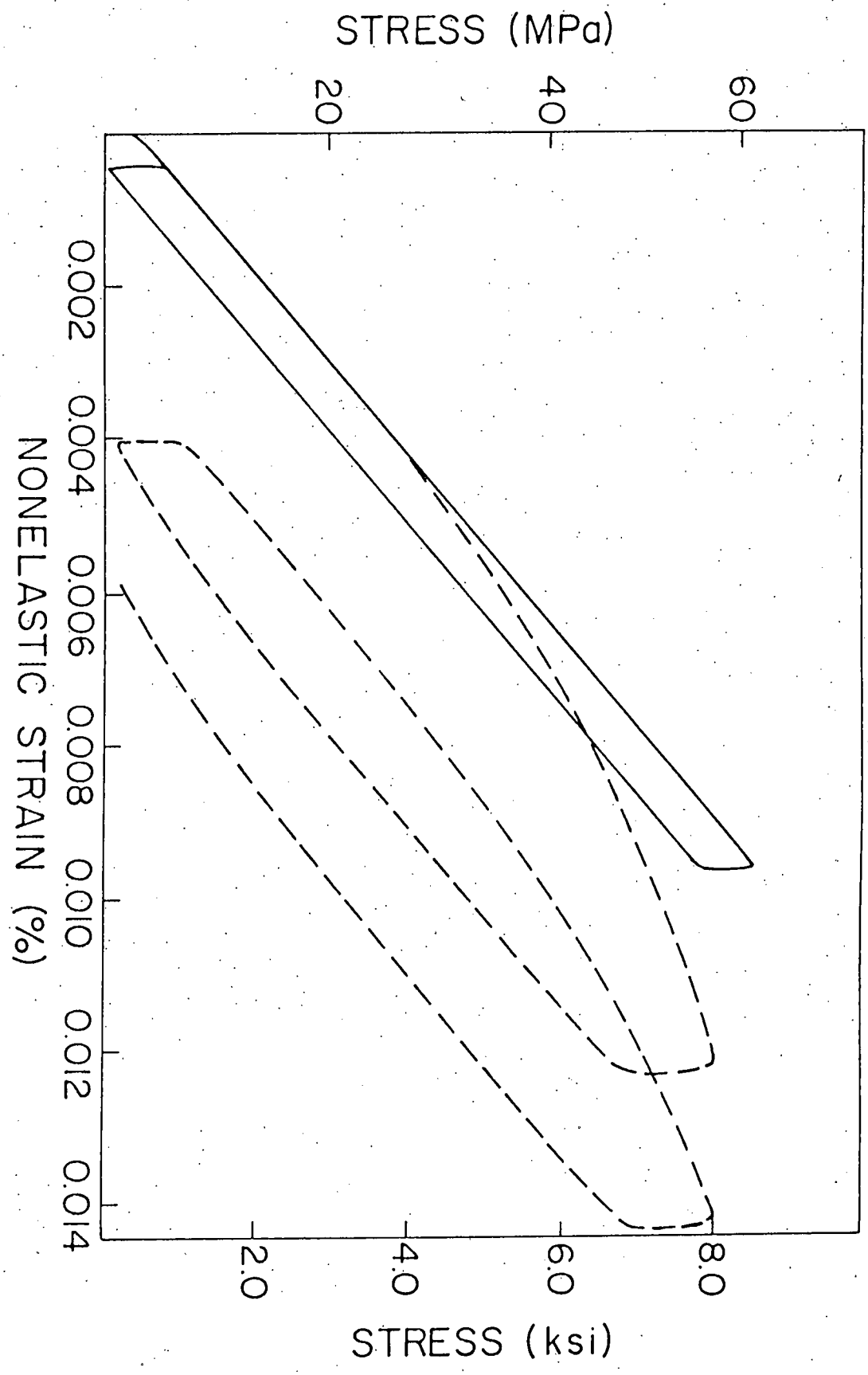
STRESS (MPa)
20
40
60
0.002
0.004
0.006
0.008
0.010
0.012
0.014
NONELASTIC STRAIN (%)
2.0
4.0
6.0
8.0
STRESS (ksi)

FIGURE 7

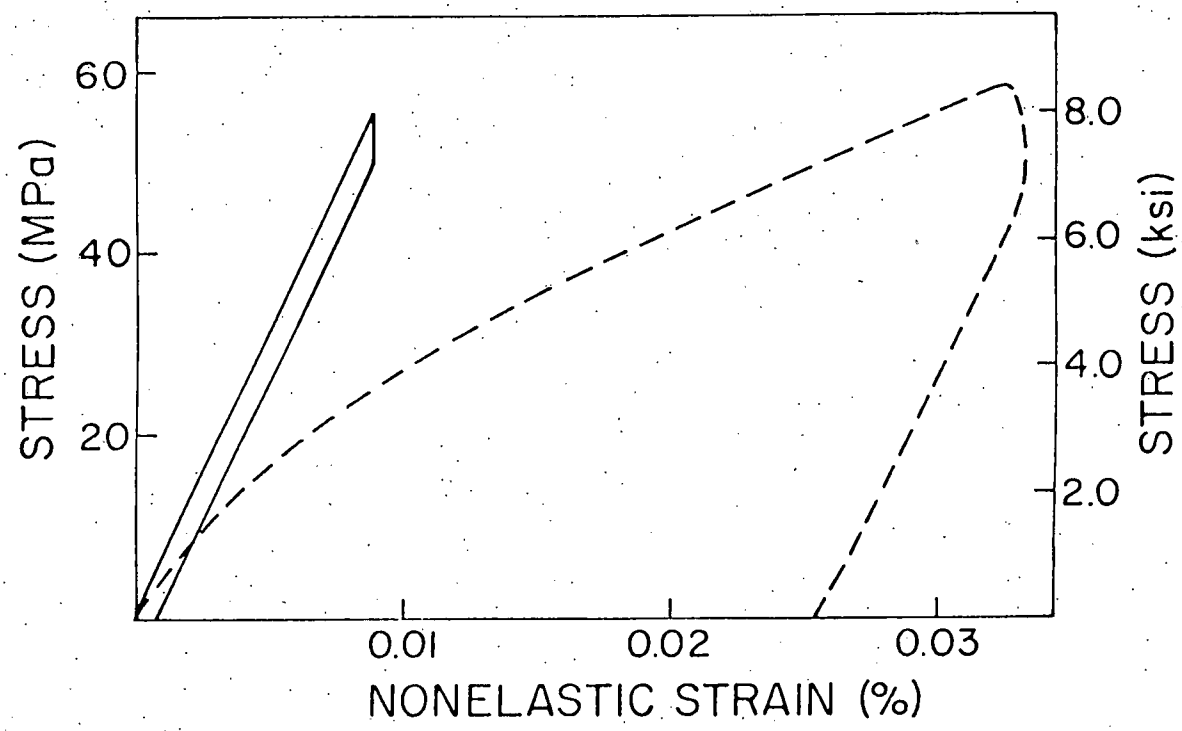
60
40
20
STRESS (MPa)
8.0
6.0
4.0
2.0
STRESS (ksi)
0.01
0.02
0.03
NONELASTIC STRAIN (%)

FIGURE 8

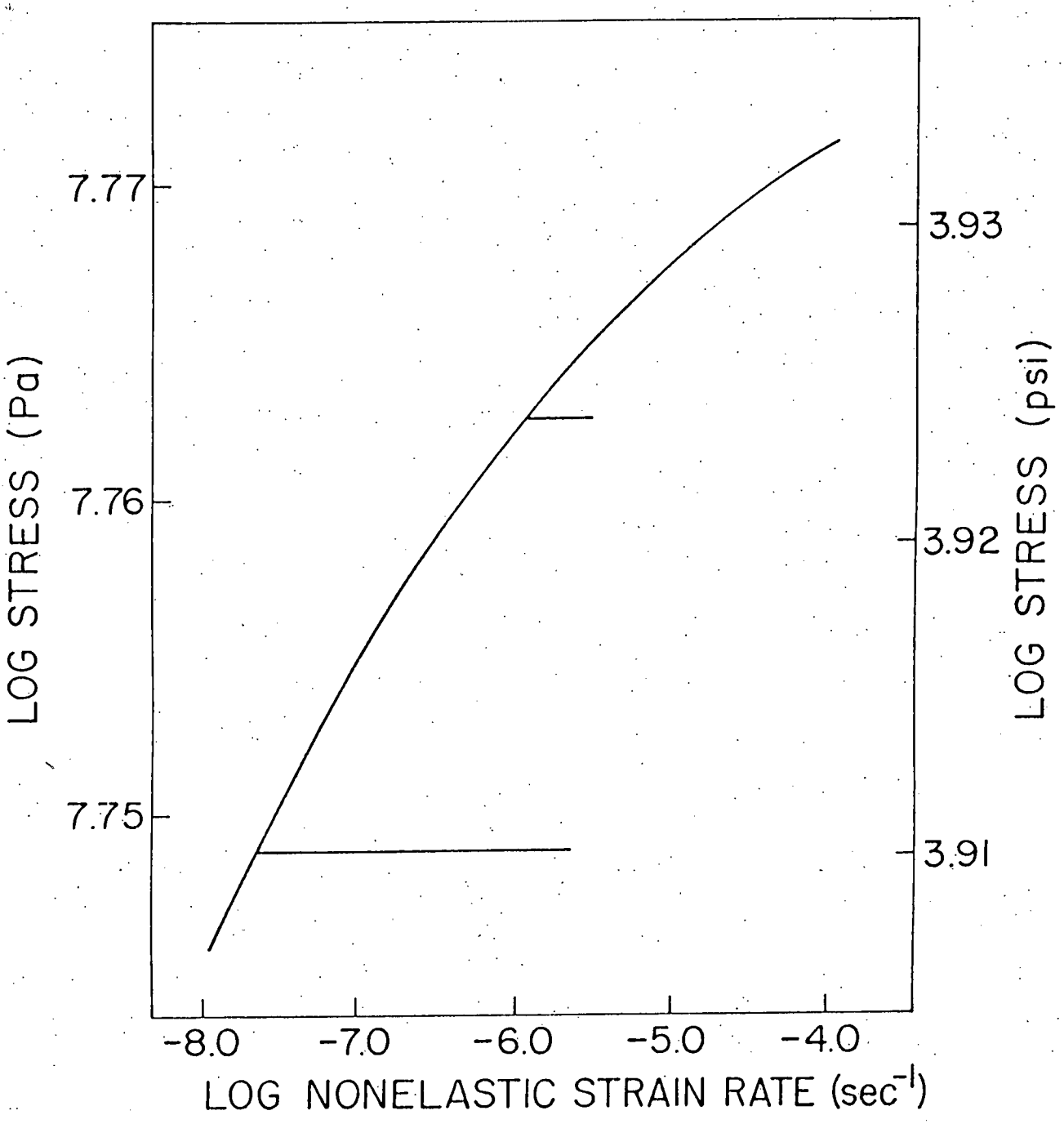
7.77
7.76
7.75
LOG STRESS (Pa)
3.93
3.92
3.91
LOG STRESS (psi)
-8.0
-7.0
-6.0
-5.0
-4.0
LOG NONELASTIC STRAIN RATE (sec^{-1})

FIGURE 9

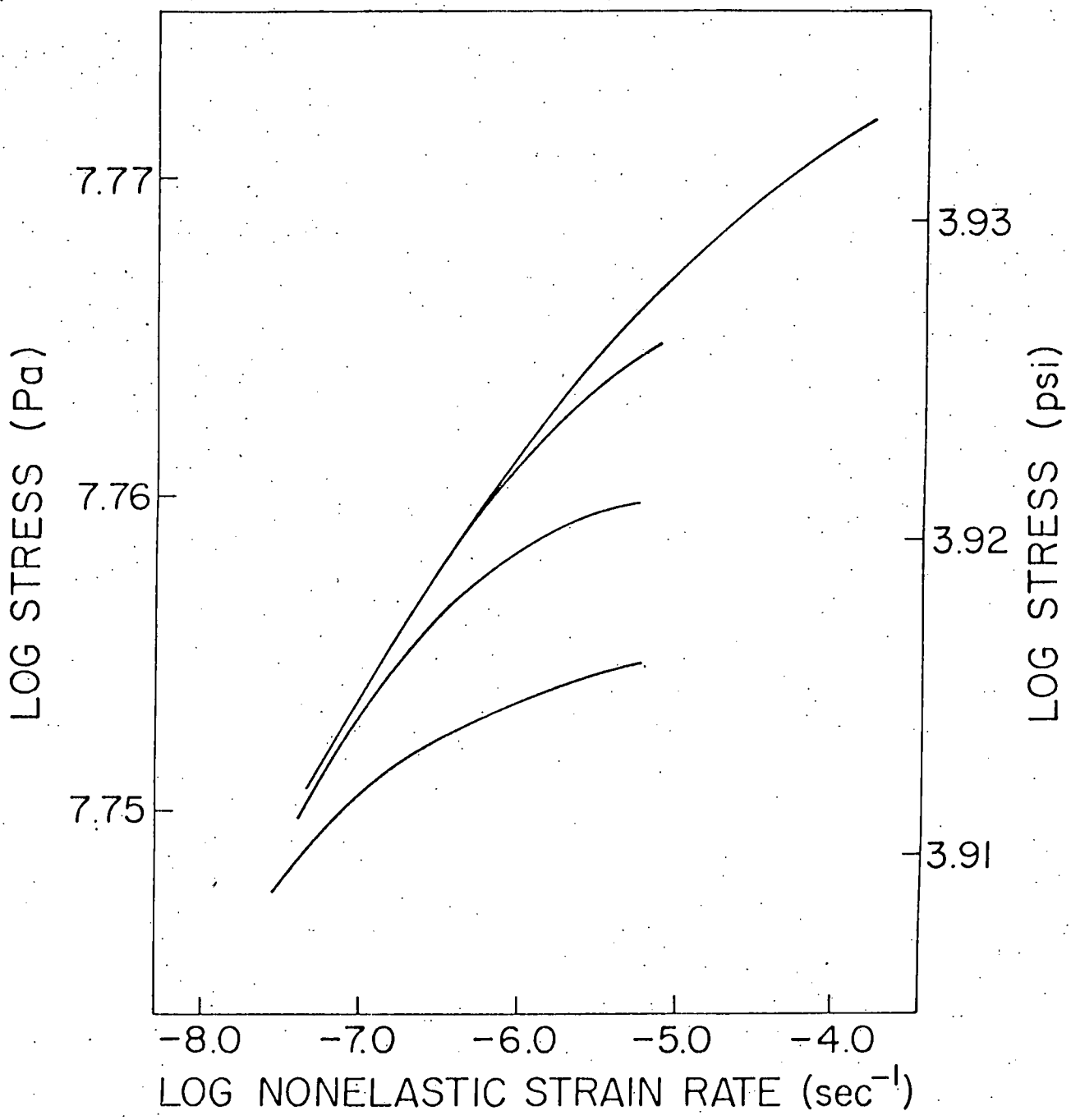
7.77
7.76
7.75
LOG STRESS (Pa)
3.93
3.92
3.91
LOG STRESS (psi)
-8.0
-7.0
-6.0
-5.0
-4.0
LOG NONELASTIC STRAIN RATE (sec^{-1})

FIGURE 10